Lindley, T. T., B. R. Bowers, G. P. Murdoch, B. R. Smith, and C. M. Gitro, 2017: Analyses of Fire-effective Low-level Thermal Ridges on the Southern Great Plains. *J. Operational Meteor.*, **5** (12), 146-160,
doi: https://doi.org/10.15191/nwajom.2017.0512


# Fire-effective Low-level Thermal Ridges on the Southern Great Plains

*T. TODD LINDLEY & BARRY R. BOWERS*
*NOAA/National Weather Service, Norman, Oklahoma*

*GREGORY P. MURDOCH*
*NOAA/National Weather Service, Midland, Texas*

*BRADLEY R. SMITH*
*Texas A&M Forest Service/Predictive Services, Austin, Texas*

*CHRISTOPHER M. GITRO*
*NOAA/National Weather Service, Pleasant Hill, Missouri*

(Manuscript received 15 February 2016; review completed 21 June 2017)

## ABSTRACT

**Low-level thermal ridges (LLTRs) have been identified as common meteorological features associated with wildfires in grass-dominated fuelscapes on the southern Great Plains. Analogous to the well-documented fire-effectiveness of West Coast thermal troughs, LLTRs on the Plains have a dramatic influence on wildland fire. Identification of these features in proximity to midlevel wind maxima has proven useful in forecasting the evolution, intensity, and areal scope of regional wildfire outbreaks. This study will provide detailed meteorological analyses of fire-effective LLTRs on the southern Great Plains. The National Centers for Environmental Prediction's North American Regional Reanalysis and National Center for Atmospheric Research Data Reanalysis are used to investigate atmospheric characteristics of LLTRs associated with 11 widespread and destructive wildfire episodes on the southern Great Plains between 2006 and 2014. Atmospheric coupling of kinematic and thermodynamic processes that influence fire effectiveness are illustrated by a vertical profile and cross section. Composites and conceptual models derived from the analyses for conflagrations on the windward side of pronounced LLTRs are used for applications in forecasting southern Great Plains wildfire outbreaks. Examples illustrating the operational utility of LLTRs in wildland fire prediction are presented. Finally, comparative observations of environments with differing fire effectiveness are shown to suggest physical influences that exacerbate surface wildland fire behavior in proximity to these atmospheric features.**

## 1. Introduction

Weather and climate ultimately control wildland fire, both through influencing build-up and conditioning of vegetative fuels as well as promoting ignition, spread, and extinction. Fundamental to the atmosphere's influence on wildland fire is the fact that hotter temperatures generally promote increased fire activity (Scott et al. 2014). Studies have described the occurrence of West Coast thermal troughs (WCTTs) as an important meteorological factor favoring wildfire growth in the Pacific Northwest (Gisborne 1927, Cramer 1954, Colson 1956, Cramer 1957, and Werth and Ochoa 1993). Brewer and Mass (2012) identified this atmospheric feature as a tongue of relatively high temperatures near the surface that extend northward along an inverted pressure trough. They also noted that, although the phenomenon has been referred to as a "thermal trough" in literature for more than a half century (in reference to its associated pressure trough, not its thermal structure), it is actually characterized by

*Corresponding author address:* T. Todd Lindley, 120 David L. Boren Blvd, Suite 2400, Norman, Oklahoma 73072
E-mail: todd.lindley@noaa.gov

a lower tropospheric thermal ridge. A modern synthesis of knowledge of extreme fire behavior defined the effects of "surface thermal troughs," referred to herein as low-level thermal ridges (LLTRs), on wildland fire as a topic of much needed research and improved understanding (Werth et al. 2016).

Research focused on wildfire outbreaks in the grass-dominated fuelscape of the southern Great Plains has similarly highlighted LLTRs (characterized by near-meridional and elongated corridors of relatively high temperatures) as important mesoscale indicators of enhanced wildfire risk (Lindley et al. 2014). Although southern plains LLTRs and WCTTs are associated with different atmospheric features (Table 1), their thermal characteristics are the same, and both present exacerbating effects on wildland fire. During particularly widespread wildfire episodes on the southern Great Plains, conflagrations frequently occur within corridors of positive temperature anomalies (Fig. 1). The most intense wildland fire activity is generally on the windward side of these anomalies where mid-tropospheric wind maxima overspread 2-m and 850-hPa thermal ridge axes from the west (Fig. 2). It was noted that spatial and temporal evolution of LLTRs and interacting wind fields aloft have predictive value in forecasting intensity and evolution of southern Great Plains wildfire outbreaks (SGPWOs, Lindley et al. 2014) (Fig. 3). Further, the lack of pronounced interaction of these features within the warm sector of passing midlatitude cyclones may reduce wildfire occurrence associated with a weather system, even in the presence of receptive vegetative fuels.

This study uses the National Centers for Environmental Prediction's (NCEP) North American Regional Reanalysis (NARR, Mesinger et al. 2006) to investigate meteorological attributes of fire-effective LLTRs associated with 11 widespread and damaging wildfire episodes on the southern Great Plains between 2006 and 2014. The NCEP/National Center for Atmospheric Research (NCAR) Reanalysis Data Composites (Kalnay et al. 1996) also are used to examine atmospheric anomalies for the presented wildfire episodes. Atmospheric analyses and 11-case composites will be shown for the diurnal burning period (1800 UTC to 2100 UTC) associated with these events. Analyses of the vertical structure of fire-effective LLTRs relative to parent midlatitude cyclones are demonstrated and illustrate atmospheric processes involved in enhancing wildland fire. The presented analyses are used to derive conceptual models for fire-effective LLTR and wind field interactions useful in operational wildland fire forecasting. When combined with a working knowledge of antecedent vegetative states and large-scale weather patterns known to support SGPWOs, conceptual models for fire-effective LLTRs are shown to be useful in predicting areas of heightened wildfire risk. Utility of these concepts is demonstrated in wildfire predictions prior to the 11 May 2014 Double Diamond Fire in Texas and damaging wildfires in Oklahoma on 24 January 2017. Finally, possible physical enhancements of the wildland fire environment induced by LLTRs will be discussed via an illustrated comparison of observed conditions within a cyclone's warm sector during the 9 April 2009 Texas and Oklahoma wildfire outbreak.

## 2. Methodology

Analyses generated using the NARR for 2-m and 850-hPa temperature and NCEP/NCAR reanalyzes for corresponding anomalies are shown to define the presented LLTRs for each of the 11 fire episodes (Table 2). Analyses of mean sea level pressure (MSLP) and anomalies, 2-m relative humidity (RH), 10-m u-wind anomalies, 500-hPa geopotential height, geopotential height anomalies, and wind also are shown to diagnose the atmospheric context of each LLTR. All NARR analyses are valid for 2100 UTC, the approximate peak of the diurnal burning period. Because of availability within the NCEP/NCAR dataset, 40-y anomalies are shown for 1800 UTC, which typically approximates the onset of the diurnal burn period. Analyses of the 11 fire-effective LLTRs utilized in the study are then composited within the NARR (NCEP/NCAR reanalysis for anomalies) to illustrate mean magnitude and relative location of common meso-α-scale thermal and kinematic atmospheric features. Conceptual models derived from these analyses are important in identifying spatial and temporal wildfire risks within synoptic-scale weather patterns known to support SGPWOs (Lindley et al. 2014).

## 3. Analyses

The meteorological environment of each presented fire-effective LLTR is analyzed below. This presentation is comprised of 12-panel figures displaying the previously indicated meteorological fields for each fire-effective LLTR case (refer ahead to Fig. 4 for formatting example). Each figure contains 11 panels showing the 2100 UTC (1800 UTC for anomalies)

**Table 1**. General comparison of southern plains LLTR and WCTT features.

| Compared Feature | Thermal Ridge | Inverted Pressure Trough | Leeside Pressure Trough | Ridge Aloft | Midlatitude Cyclone | Downslope | Duration |
|---|---|---|---|---|---|---|---|
| LLTR | Yes | No | Yes | No | Yes | Yes | 1–2 Days |
| WCTT | Yes | Yes | No | Yes | No | Yes | 1–5 Days |

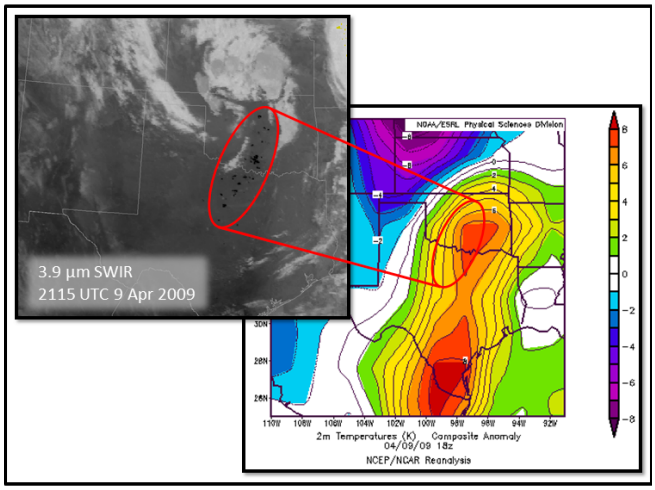


**Figure 1**. NCEP/NCAR 2-m temperature anomalies at 1800 UTC 9 April 2009 and 2115 UTC 9 April 2009 from GOES shortwave infrared (SWIR, 3.9 µm) satellite-detected wildfires collocated with corridor of above-normal temperatures. *Click image for an external version; this applies to all figures hereafter.*

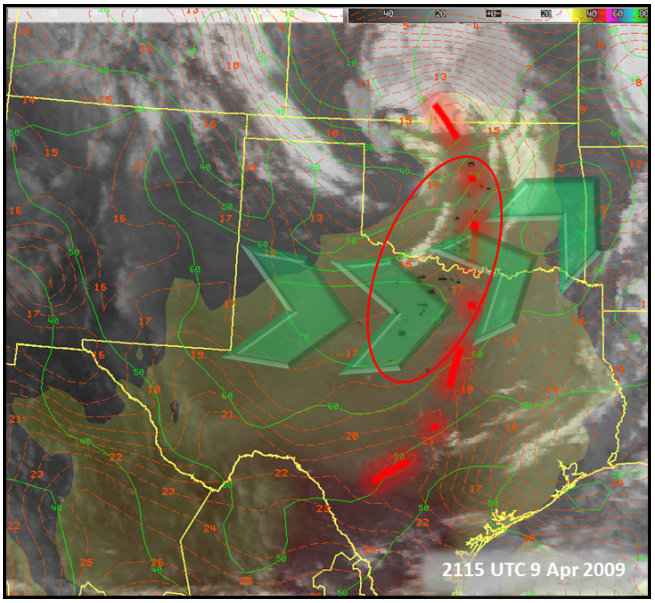


**Figure 2**. GOES shortwave infrared (3.9 µm) from 2115 UTC 9 April 2009 illustrating juxtaposition of LLTR (red dashed line) and overspreading midlevel wind maximum (green arrows) with satellite-detected wildfires (circled in red). Also shown are 850-hPa isotherms (thin, red, dashed contours), 500-hPa isotachs (green solid contours), and 2-m temperatures ≥30° C (light yellow area on image).

analysis for the specified field. The twelfth panel (lower right) contains an 11-case composite for the specified atmospheric parameter. Both 2-m and 850-hPa thermal ridge axes are demarked and collectively constitute the low-level thermal ridge. To initially define LLTR axes associated with each fire case, analyses of 2-m and 850-hPa temperatures and anomalies are shown first. It is important to note, however, that the presented analyses represent an instantaneous picture, or "snap shot," of the depicted features valid at 2100 UTC (1800 UTC for anomalies). All the analyzed atmospheric features, including the LLTR and its fire-effective conditions, evolve and translate (generally from west to east) throughout the diurnal burning period. This analysis focuses on the common meteorological attributes of each fire-effective LLTR. It is imperative to note that the most striking common attribute is that wildfires generally occur within an area bounded by the mid-tropospheric (500-hPa) wind maximum to the west and the LLTR to the east. It is the interaction of the overspreading wind maxima aloft that defines and promotes fire-effectiveness of LLTRs in a fire-favorable vegetative environment.

Analyses of 2-m temperatures show pronounced thermal ridges that span a west-to-east distance of 150–

**Table 2**. Summary of wildfire impacts related to the 11 fire-effective LLTR episodes analyzed in this study.

| Date | # of Fires | Burn Area | Structures Lost | Fatalities | Injuries |
|---|---|---|---|---|---|
| 12 Mar 2006 | 27 | 4459.8 km$^2$ | 102 | 12 | 11 |
| 15 Apr 2006 | 10 | 93.6 km$^2$ | 7 | 0 | 3 |
| 4 Apr 2009 | 23 | 136.9 km$^2$ | 35 | 1 | 35 |
| 9 Apr 2009 | 29 | 954.2 km$^2$ | 339 | 4 | 62 |
| 27 Feb 2011 | 39 | 1153.0 km$^2$ | 210 | 1 | 4 |
| 22 Mar 2011 | 20 | 282.9 km$^2$ | 10 | 0 | 2 |
| 9 Apr 2011 | 22 | 446.1 km$^2$ | 87 | 1 | 3 |
| 14 Apr 2011 | 36 | 329.7 km$^2$ | 70 | 1 | 10 |
| 24 May 2011 | 16 | 302.0 km$^2$ | 9 | 0 | 2 |
| 20 Jun 2011 | 19 | 234.7 km$^2$ | 5 | 0 | 3 |
| 11 May 2014 | 1 | 10.5 km$^2$ | 225 | 1 | 0 |

300 km in each of the 11 cases (Fig. 4). This narrow temperature ridge also is well-depicted at the same scale in the 11-case composite. Observed 2-m temperatures along the thermal ridges generally range from 25°C to 40°C, while 2-m temperature anomalies range between +4°C and +16°C (Fig. 5). Additionally, most of the cases show very pronounced thermal ridges in the 850-hPa temperature analyses, with temperatures between 15°C and 30°C (Fig. 6) and 850-hPa anomalies between +2°C and +16°C (Fig. 7). The 9 April 2009 case is analyzed as a relatively weaker thermal ridge suppressed by cold air advection over the High Plains of western Texas, but the associated corridor of warmer temperatures was more pronounced in the 2-m temperature analysis. The signal for the 9 April 2009 LLTR is better depicted in 2-m and 850-hPa temperature anomalies, where 2-m anomalies of +6°C to +8°C are indicated. In fact, broad meridional corridors of positive low-level temperature anomalies with west-to-east spans of 500–800 km are characteristic of all the presented fire-effective LLTRs.

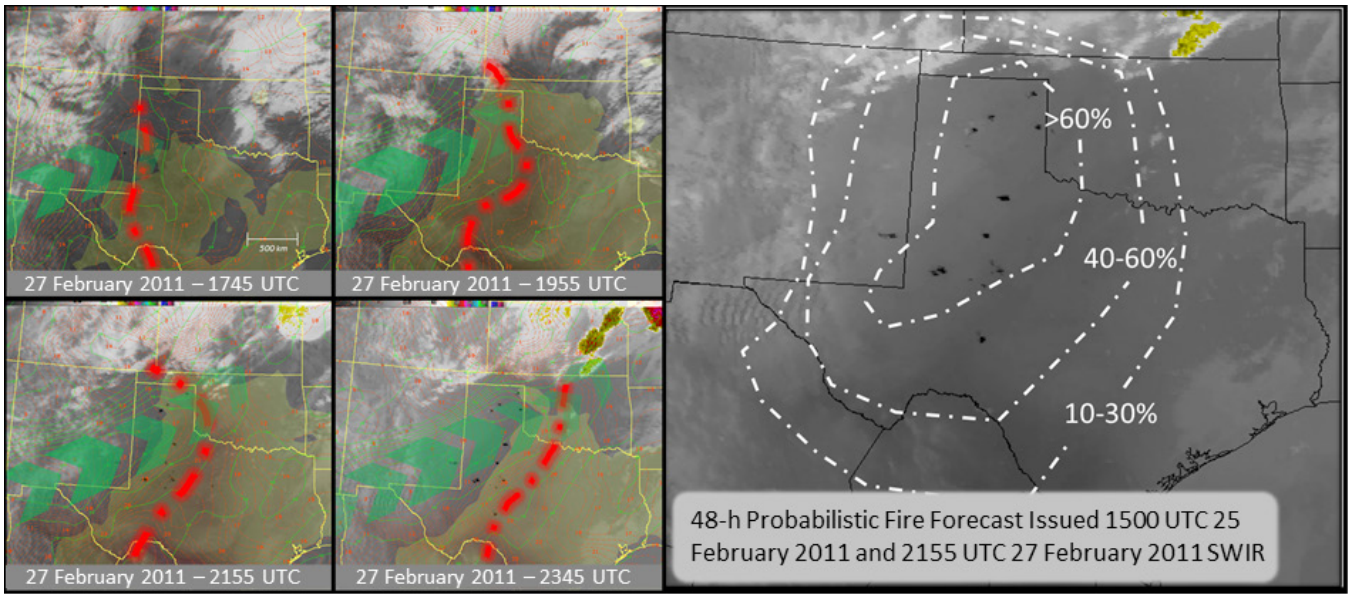


**Figure 3**. Evolution of LLTR (red dashed line), and 2-m temperatures ≥30° C (yellow area on image), midlevel wind maximum (green arrows) between 1745 UTC and 2345 UTC 27 February 2011 (left) and experimental 48-h probabilistic wildfire forecast (right) issued 1500 UTC 25 February 2011 based on numerical weather predictions of this evolution shown with 2155 UTC 27 February 2011 shortwave infrared satellite-detected wildfires (black spots).

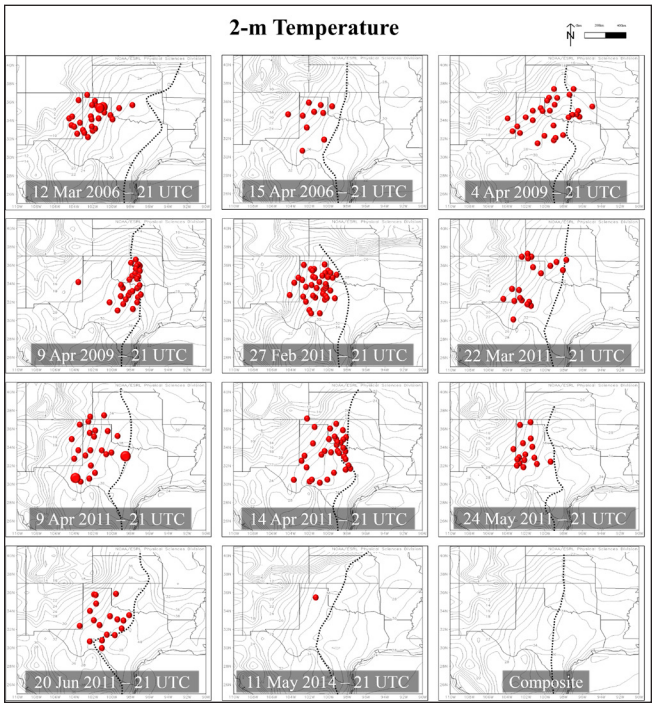


**Figure 4**. NCEP/NARR analysis and composite 2-m temperatures for the 11 fire-effective LLTR cases. The 2-m temperature ridge axis is denoted as a short hatched black line here and in subsequent analyses. Fire locations indicated (red dots), with fires ≥404 km$^2$ (1000 acres) noted (larger red dots) here and in subsequent figures.

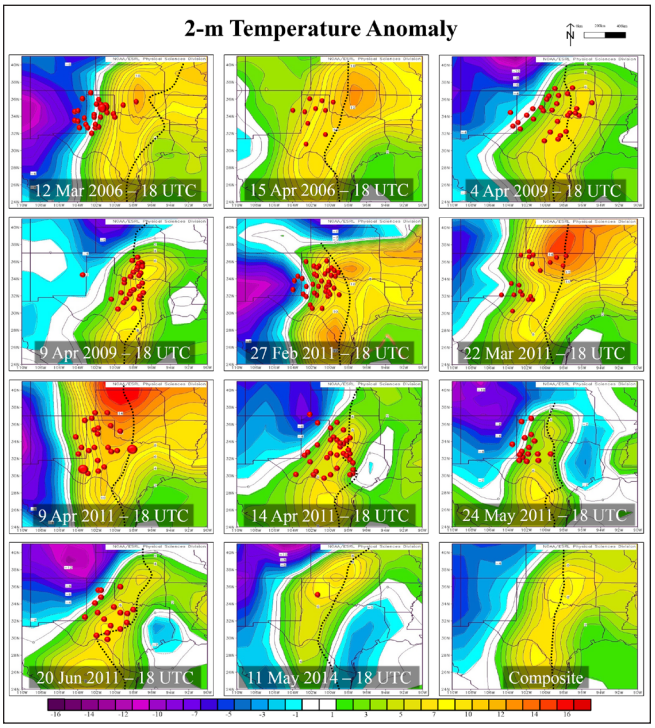


**Figure 5**. NCEP/NCAR analyses and composite 2-m temperature anomalies for the 11 fire-effective LLTR cases.

A strong signal associating southern Great Plains fire-effective LLTRs to surface pressure troughs is evident in MSLP analyses. All the presented LLTRs are

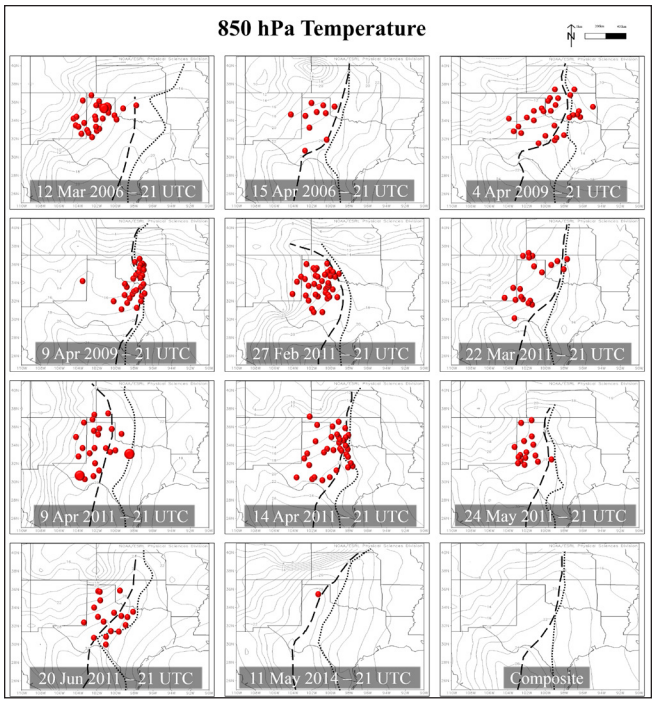


**Figure 6**. NCEP/NARR analysis and composite 850-hPa temperatures for the 11 fire-effective LLTR cases. The 850-hPa temperature ridge axis is denoted as a long, hatched black line here and in subsequent analyses.

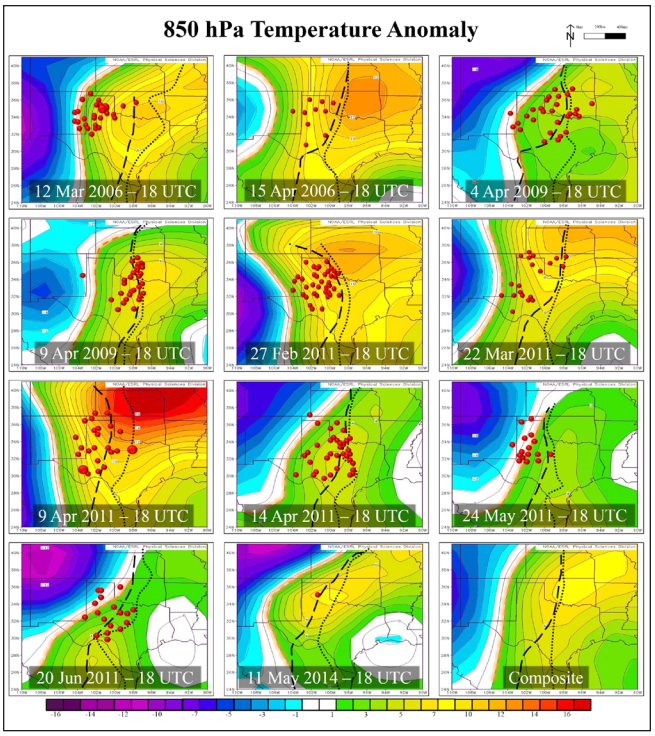


**Figure 7**. NCEP/NCAR analyses and composite 850-hPa temperature anomalies for the 11 fire-effective LLTR cases. The windward periphery of positive 850-hPa temperature anomalies is denoted as an orange dashed line here and in subsequent analyses.

coincident with 994-hPa to 1004-hPa MSLP troughs (Fig. 8) and deeply negative MSLP anomalies of –10 hPa to –20 hPa (Fig. 9). This illustrates that fire-effective LLTRs on the southern Great Plains closely reflect MSLP trough axes and are consistent with conceptual models for lee surface pressure troughs indicative of downslope flow and adiabatic warming (Steenburgh and Mass 1994 and Hobbs et al. 1996). As such, surface troughs associated with LLTRs generally result from lee cyclogenesis (Pierrehumbert 1986) and differ from those associated with WCTTs, which instead are "inverted" as described in numerous studies (Miller 1946, Baker 1971, Bosart et al. 1972, Bosart 1975, Ballentine 1980, Richwien 1980, Bosart 1981, Forbes et al. 1987, Keshishian and Bosart 1987, Bell and Bosart 1988, Doyle and Warner 1990, Keshishian et al. 1994, Weisman et al. 2002, and Schumacher et al. 2008).

Fire-effective LLTRs on the southern Great Plains frequently occur in proximity to strong surface moisture gradients. Analyses of 2-m RH for the 11 LLTR cases show that both the 2-m and 850-hPa thermal ridges are closely tied to transitional boundaries of dry and moist air masses within the cyclone's warm sector (Fig. 10) or drylines (Carlson and Ludlam 1968, Schaefer 1973, Peterson 1983, and Schaefer 1986). This is characteristic of the traditionally recognized "dryline regional critical fire weather pattern" for the southwestern United States (Werth et al. 2011). A notable attribute of this analysis is that the thermal ridge occurs along the low-level moisture gradient and not in the core of the dry air mass where relatively lower dewpoint temperatures exist (not shown). Fire-effective LLTRs are generally shown to be displaced east of the core of lowest RH. Lindley et al. (2014) noted that intense fire conflagrations tend to favor areas along and windward of LLTRs in zones of positive temperature anomalies, and frequently, minimum fire activity occurs within the core of the dry air mass where lower RH, lower temperature, and higher wind environments exist west of LLTRs. This demonstrates an apparent physical dependency of critical wildland fire processes on the relatively higher temperature environments along LLTRs that contributes more to fire-effectiveness than RH and wind alone. Werth et al. (2016) related critical fire weather to an onset of strong southwesterly winds, sudden decreases in RH, and rapidly drying fuels in association with dryline passages. It is important to note, however,

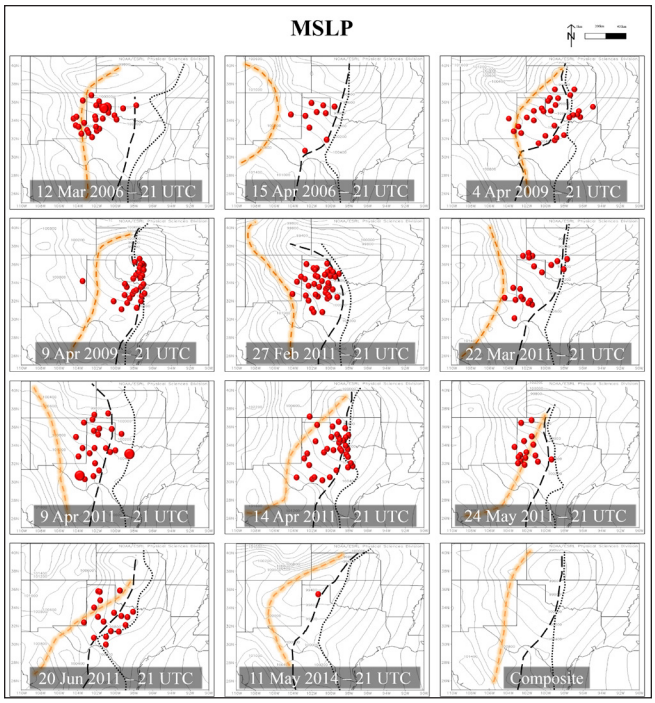


**Figure 8**. NCEP/NARR analysis and composite MSLP for the 11 fire-effective LLTR cases.

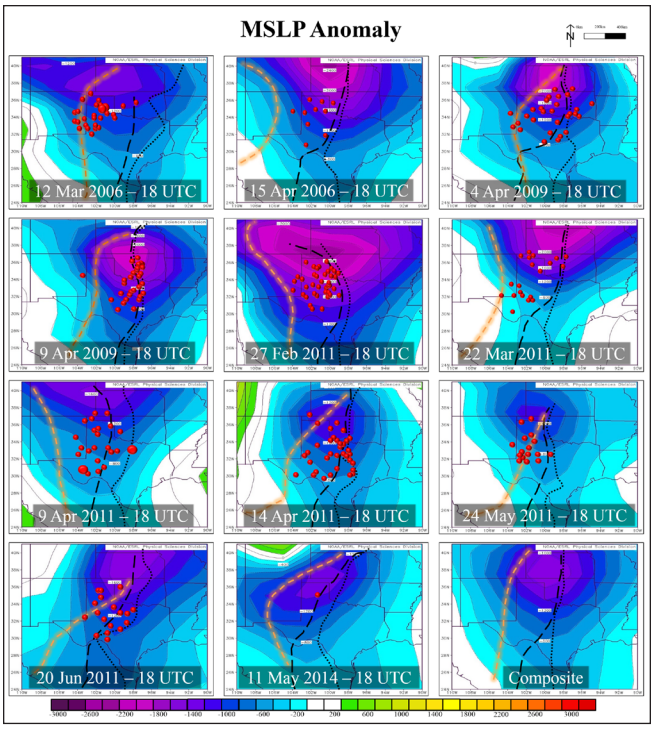


**Figure 9**. NCEP/NCAR analyses and composite MSLP anomalies for the 11 fire-effective LLTR cases.

that although LLTRs are commonly a component of dryline structure (Schaefer 1986), anomalously high temperatures along LLTRs contribute more to wildland fire processes than dryline-induced moisture gradients. In fact, observations of some fire-effective LLTRs have occurred in the absence of an analyzed dryline.

Analyzed fire-effective LLTRs occurred on average approximately 500 km east of 500-hPa geopotential height troughs axes or lows (Fig. 11). In general, LLTRs were located beneath southwesterly to westerly midlevel flow to the east or southeast of shortwave trough axes, usually on the southeastern periphery of negative 500-hPa geopotential height anomalies (Fig. 12). This is consistent with past research on wildfire "crisis periods," which concluded that the greatest danger is commonly east of upper air troughs in areas of low surface pressure (Syverson 1963). The 9 April 2011 LLTR represents a minor deviation from this commonality and instead occurred within positive geopotential height anomalies well downstream of the approaching 500-hPa geopotential height trough. This particular thermal ridge was spatially broad with the central axis displaced approximately 600 km east of upstream negative geopotential height anomalies and nearly 1000 km in advance of the approaching 500-hPa trough axis. The western periphery of an expansive area of positive low-level temperature anomalies extended westward beneath a strong geopotential height anomaly gradient. Although this case was characterized by a greater spatial separation of the midlevel geopotential height trough axis and the LLTR, the overall pattern is consistent with all the cases presented.

Interaction of strong wind fields with anomalously warm temperatures associated with LLTRs appears to be a critical contributor to fire-effectiveness. All the analyses indicate that LLTR axes occurred along and east of *u*-component 10-m wind fields with anomalies of +6 m $s^{-1}$ to +12 m $s^{-1}$ (Fig. 13). A more operationally useful way to illustrate the role of strong winds overspreading LLTRs is seen in analyses of 500-hPa wind (Fig. 14). This signal is well-depicted in the 11-case composite with the LLTR oriented roughly north-to-south immediately east of the 500-hPa wind maximum. All the presented cases show the nose, or exit region, of pronounced mid-tropospheric wind maxima with 500-hPa speeds between 45 m $s^{-1}$ and 55 m $s^{-1}$ overspreading positive temperature anomalies west of LLTR axes. Conditions favorable for wildfires typically occur on the windward side of positive temperature anomalies and LLTRs along or near the axis of the overspreading midlevel jet. These meso-α-scale atmospheric features are frequently depicted with a high degree of predictability in numerical weather

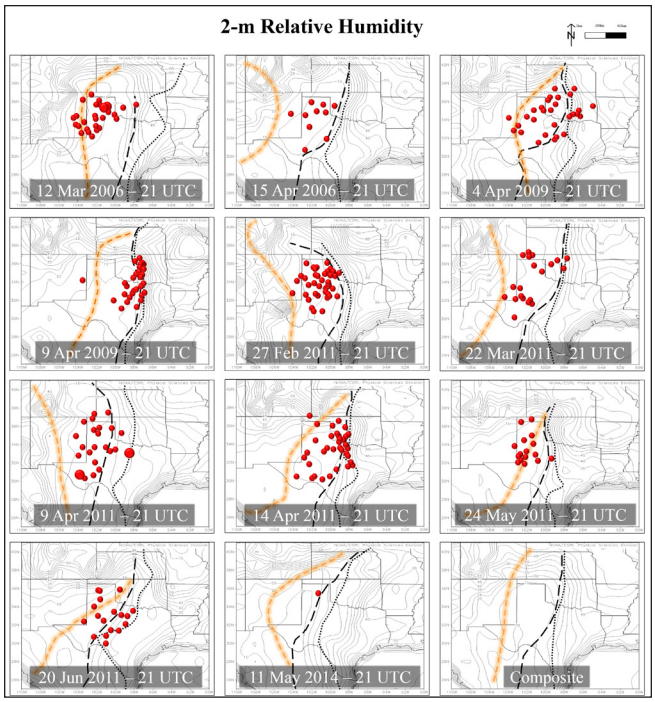


**Figure 10**. NCEP/NARR analysis and composite 2-m RH for the 11 fire-effective LLTR cases.

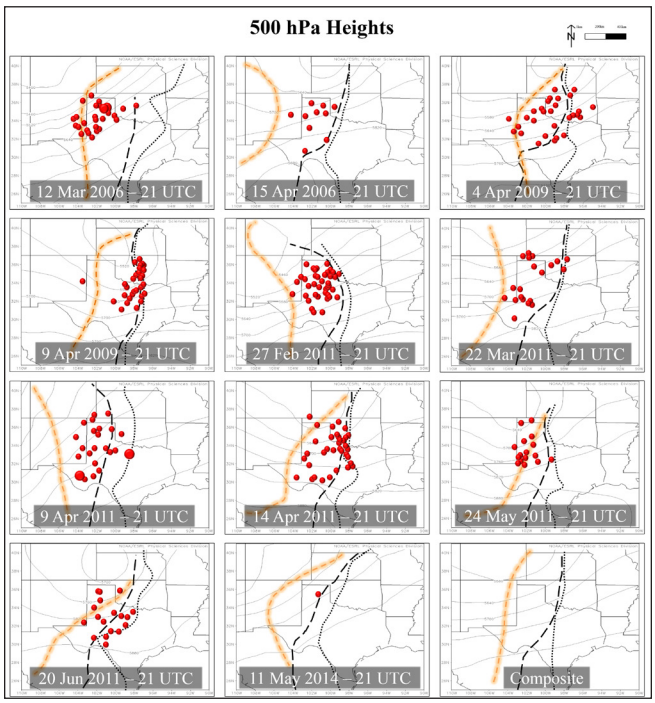


**Figure 11**. NCEP/NARR analysis and composite 500-hPa geopotential heights for the 11 fire-effective LLTR cases.

models. Thus, identification of interacting LLTRs and wind maxima aloft has led to improved forecasts and warnings for high-impact wildfire episodes on

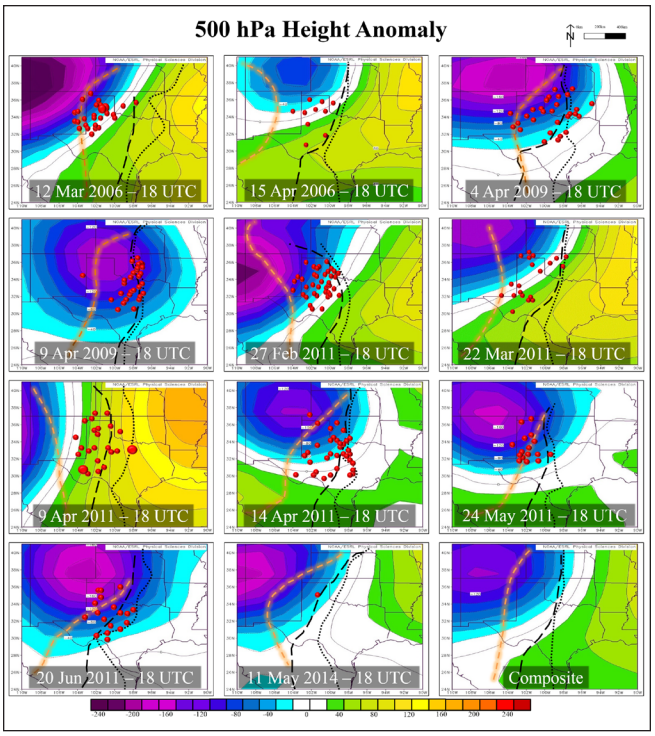


**Figure 12**. NCEP/NCAR analyses and composite 500-hPa geopotential height anomalies for the 11 fire-effective LLTR cases.

the southern Great Plains (Lindley et al. 2014). A composite atmospheric sounding for the 11 presented LLTR cases derived from North American Mesoscale Binary Unformatted Format for the Representation of meteorological data (NAM BUFR) for points within the fire-effective areas suggests vertical mixing of the planetary boundary layer is likely enhanced by anomalously warm temperatures along the LLTR (Fig. 15). The enhanced depth of vertical mixing (upwards of 700-hPa per the composite sounding) increases the transfer of strong winds aloft toward the surface.

Atmospheric processes associated with fire-effective LLTRs are perhaps best illustrated via a vertical cross section. On 6 March 2017, a particularly violent firestorm incinerated nearly 5000 km$^2$ along a fire-effective LLTR on the southern Great Plains of Texas, Oklahoma, and Kansas. A Rapid Refresh (RAP, Benjamin et al. 2016) west-to-east cross section along a line from near Tierra Amarilla, New Mexico, to near Carney, Kansas, sampled the fire zone between the 500-hPa wind maximum and the LLTR over southwestern Kansas and northwestern Oklahoma (Fig. 16). This cross section depicted strong winds flowing along downward sloping isentropic surfaces on the windward side of the LLTR (Fig. 17). The depicted isentropes

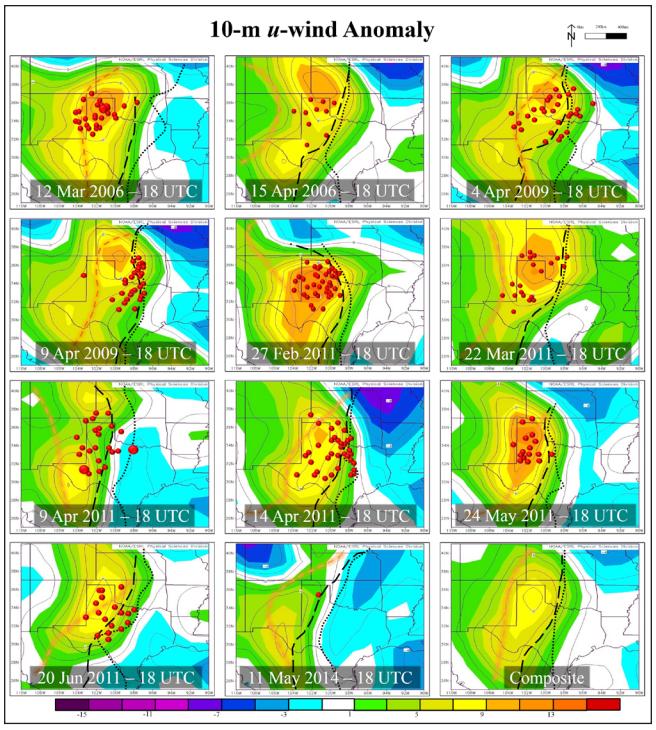


**Figure 13**. NCEP/NCAR analyses and composite 10-m u-wind anomalies for the 11 fire-effective LLTR cases.

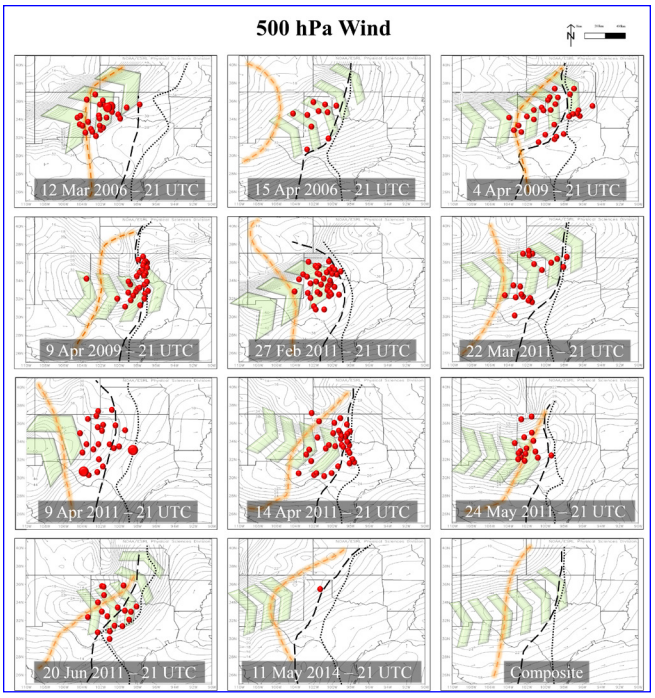


**Figure 14**. NCEP/NARR analysis and composite 500-hPa wind speed for the 11 fire-effective LLTR cases. Maximum wind speeds are denoted with green arrows. Arrow size here and in subsequent analyses correlates to maximum wind speeds in the 30 m $s^{-1}$ range (small), 40 m $s^{-1}$ range (medium), and 50 m $s^{-1}$ range (large).

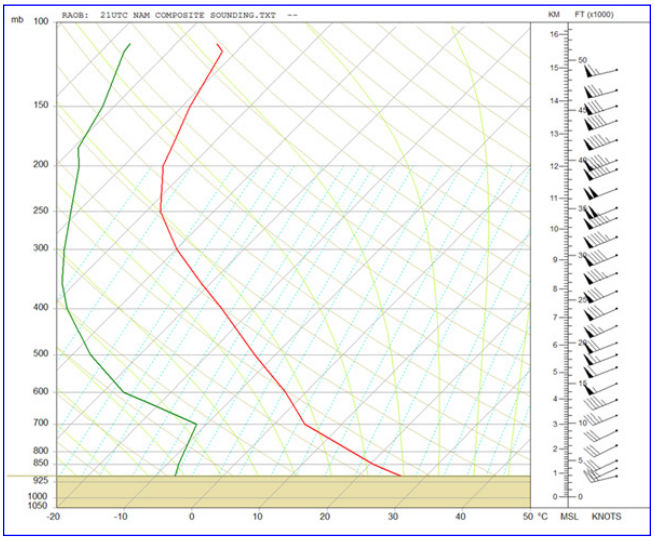


**Figure 15**. Composite NAM BUFR sounding representative of the burn area for each of the 11 LLTR cases presented.

sharply intersected the surface within a corridor of dry adiabatic low-level temperature lapse rates along the LLTR. Winds >25 m $s^{-1}$ are shown transferring toward the ground within the deeply mixed planetary boundary layer of the LLTR. Isentropic surfaces jump vertically immediately east of the LLTR where strong gradients in low-level lapse rates exist. The 6 March 2017 fire-effective LLTR cross section demonstrates how wind-driven wildfire on the Plains is truly a dry convective process that couples atmospheric thermal and kinematic processes with the surface through the culmination of biospheric responses to climate, seasonal variation, and weather.

Within the 11-case dataset presented, variations in orientation of LLTRs and overspreading wind maxima are evident. These variations in relative spatial configuration of thermal and kinematic features appear to influence the overall scope and geographical area of enhanced wildfire threat and are categorized here by three conceptual model types (Fig. 18). The Type A conceptual model for fire-effective LLTRs on the southern Great Plains features a wind maximum aloft that overspreads a narrow LLTR with an approximate normal angle of incidence. This type of fire-effective LLTR is typically highly amplified and results in a focused area of intense fire-effectiveness near the intersection of these atmospheric features. From the cases presented in this study, 9 April 2009, 14 April 2011, and 24 May 2011 are examples of Type A fire-effective LLTRs.

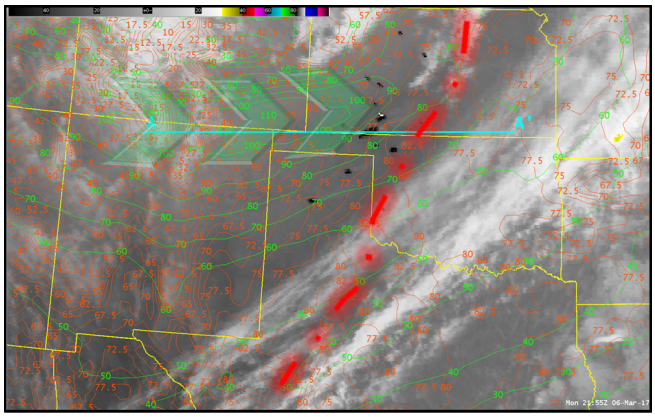

**Figure 16**. Shortwave infrared with detected wildfires (black splotches) at 2155 UTC 6 March 2017 with RAP-analyzed 2-m temperature (red dashed isotherms, °F), 2-m LLTR (heavy, red dashed line), 500-hPa wind speed (green solid isotachs, kt), 51–57 m $s^{-1}$ (100–110 kt) wind maximum (green arrows), and line denoting the Fig. 17 cross-sectional area (cyan line A–A').

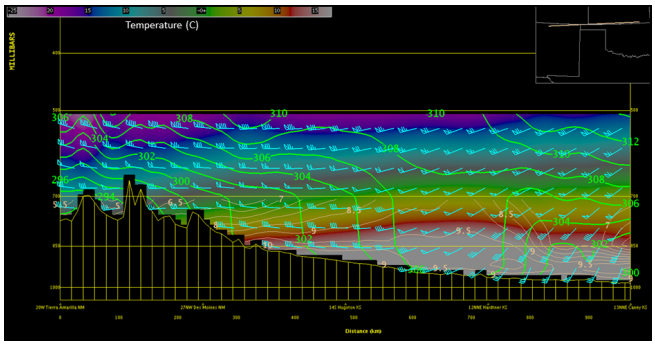


**Figure 17**. RAP vertical cross section along line A–A' depicted in the previous figure (Fig. 16) from 2200 UTC 6 March 2017 showing potential temperature (green isentropes, °K), wind (cyan barbs), temperature lapse rate (tan contours, °C), and temperature (colored bands in image, °C).

The most common meso-α-scale configuration for fire-effective LLTRs is illustrated here as Type B. A Type B fire-effective LLTR on the southern Great Plains is indicated by a relatively narrow and highly amplified LLTR overspread by a midlevel wind maximum embedded within southwesterly flow aloft that intersects the LLTR at an angle of incidence of approximately 45°. In the case of a Type B fire-effective LLTR, fire-effective conditions are bounded by the axis of the midlevel wind maximum where it overspreads the periphery of positive temperature anomalies to the west and the LLTR axis to the east. Examples of the Type B fire-effective LLTR from the presented dataset include 12 March 2006, 15 April 2006, 4 April 2009, 27 February 2011, 22 March 2011, 20 June 2011, and 11 May 2014.

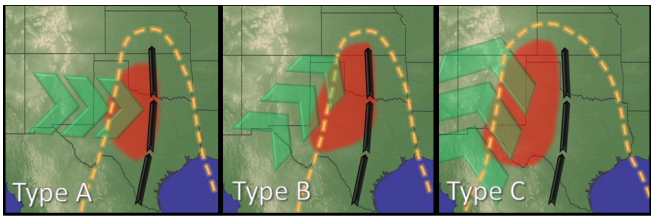


**Figure 18**. Conceptual models for three configurations of interacting wind fields aloft and LLTRs that are fire-effective on the southern Great Plains. Shown are 500-hPa wind maximum (green arrows, Type A and B generally 30 m $s^{-1}$ to 40 m $s^{-1}$, Type C 50 m $s^{-1}$), LLTR axis (black arrows), and periphery of positive 850-hPa temperature anomalies (orange dashed line).

The least common fire-effective interaction of wind fields aloft and LLTRs is referenced here as Type C. This is characterized by a broad but highly amplified LLTR with increasingly strong near-meridional flow overspreading the LLTR from the west. This configuration of favorable thermal and kinematic features results in an expansive area of fire-effective conditions bounded by the periphery of positive low-level temperature anomalies to the west and the LLTR axis to the east. This scenario generally occurs in advance of approaching midlatitude shortwave troughs and is most fire-effective during periods of exceedingly volatile vegetative fuel conditions (Lindley et al. 2014). The 9 April 2011 fire-effective LLTR presented in this study represents a Type C fire-effective thermal ridge. Although less common, the widespread nature of fire-effective conditions associated with this configuration presents a notable hazard.

It is important to note that, given a fire-prone antecedent state of vegetative fuels, any of the described Type A–C variant configurations of interacting wind fields and LLTRs are fire-effective atmospheric patterns. Recognition of fire-effective LLTR type, as noted, may provide some degree of predictability to the overall magnitude and scope of an anticipated wildland fire episode.

## 4. Discussion

### *a. LLTR structure and relation to SGPWOs*

Unlike the well-documented WCTT, which is associated with geopotential height ridges aloft, fire-effective LLTRs on the Plains are manifested as leeside

troughs associated with the passage of midlatitude cyclones. The 11-case composite analyses of 500-hPa geopotential heights, 850-hPa temperature, 2-m temperature, 2-m RH, and MSLP are used to construct a conceptual model for fire-effective LLTRs relative to parent midlatitude cyclones (Fig. 19). This visualization illustrates the vertical structure of the collective LLTR, which occurs beneath southwesterly flow aloft in advance of or in close proximity to a shortwave trough axis and is in close spatial proximity to the MSLP trough axis. It is important to note that the LLTR also occurs along a low-level moisture gradient, or dryline. Therefore, the core of dry air within the warm sector of the parent cyclone is displaced west of a fire-effective LLTR.

Ten of the 11 LLTR cases presented in this study were associated with SGPWOs. Only the 11 May 2014 Double Diamond Fire case represents an individual and localized high-impact wildfire event. The fire-effective LLTR is a key feature of the SGPWO phenomenon and its atmospheric composite. For use in operational forecasts and warnings, knowledge of the fire-effective LLTR is vital for identifying specific geographical areas of heightened wildfire risk within the broader synoptic-scale SGPWO composite pattern.

### b. *Examples of forecast utility*

An example application of fire-effective LLTR recognition in operational wildland fire prediction is illustrated by the Storm Prediction Center (SPC) Day 2 Fire Weather Outlook issued at 1857 UTC 10 May 2014. In this outlook, the SPC forecaster cited identification of low- to midlevel wind maxima interacting with an LLTR as justifying a "high-end fire weather threat" forecast and upgraded the outlook to "Extremely Critical" over a geographically small area of the central Texas Panhandle. On 11 May 2014, the Double Diamond Fire destroyed 225 homes near Fritch, Texas (Fig. 20). In this example, the SPC forecaster explicitly discussed the fire-effective LLTR as reasoning for a precise, high-end, wildland fire forecast.

Subsequent wildland fire predictions using recognition of fire-effective LLTRs also have demonstrated operational success. An Area Forecast Discussion from the National Weather Service Weather Forecast Office in Norman, Oklahoma, issued on 24 January 2017 cited 36 m $s^{-1}$ midlevel winds expected to "intersect with a low level thermal ridge…oriented north to south across central Oklahoma…a pattern recognized for significant fire potential." This reasoning was used

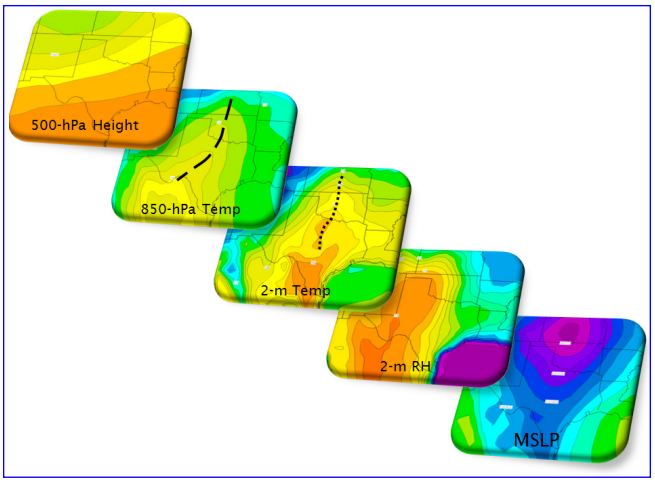


**Figure 19**. Diagram showing the composite location of the 2-m and 850-hPa thermal ridge axes relative to midlatitude geopotential height, RH, and MSLP fields within a parent midlatitude cyclone.

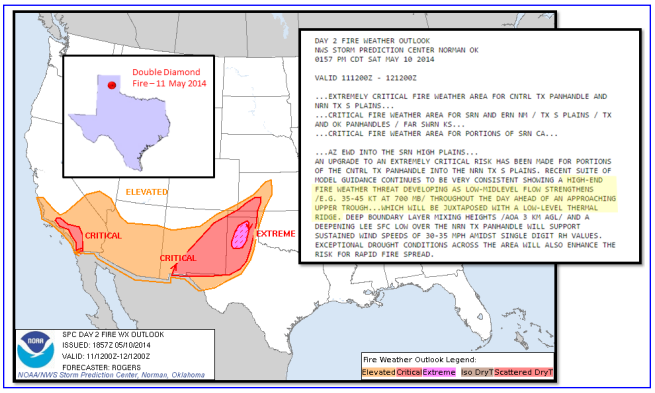


**Figure 20**. Recognition of the use of a fire-effective LLTR in an SPC Fire Weather Outlook prior to the devastating 11 May 2014 Double Diamond Fire in Texas.

to justify Red Flag warnings where combinations of RH and wind speed did not technically meet traditional warning criteria in advance of damaging wildfires that destroyed homes in Logan County, Oklahoma.

### c. *LLTR influence on fire environment*

Jensen and McPherson (2008) stated that hotter weather makes fuels more combustible, and although this is intuitive, the physical influence of LLTRs on the fire environment is not fully understood. Although a conclusive determination of the exact causative processes involved in promoting problematic wildland fire along LLTRs is beyond the scope of this paper, the 9 April 2009 wildfire outbreak is used to illustrate differences in the meteorological fire environment

of the LLTR relative to conditions in the core of the warm sector's dry air mass located farther to the west. Data from the Realtime Observation Monitoring and Analysis Network (ROMAN, Horel et al. 2004) Remote Automated Weather System (RAWS) at Midland, Texas (MAF), sampled conditions in the core of the dry air mass approximately 460 km west-southwest of the fire outbreak, while data from the LBJ Road, Texas (LBJ), RAWS were in proximity to the fire-effective LLTR (Fig. 21).

A plot of sustained 6-m wind speeds at MAF and LBJ shows that winds were considerably stronger in the core of the dry air at MAF than those within the LLTR at LBJ (Fig. 22). Maximum sustained wind speeds at LBJ during the period of the fire outbreak reached 8 m $s^{-1}$ at 2000 UTC 9 April 2009. Sustained winds were 10.7 m $s^{-1}$ at MAF with a peak of 14.3 m $s^{-1}$ at 1700 UTC 9 April 2009. In addition, 2-m relative humidity data show a decrease in moisture during the diurnal burn period at LBJ, with minimum RH values of 6% between 2000 UTC and 2100 UTC on 9 April 2009 (Fig. 23). Of particular note is the dramatic drop in RH observed at LBJ as the LLTR amplified over the region at the onset of the diurnal burn period between 1800 UTC and 1900 UTC, with RHs falling from 50% to 9% within the 1-h period. Although the magnitude of drying was greatest in proximity to the LLTR, equally dry air extended far westward into the core of the dry air mass. Daytime minimum RH values also reached 6% at MAF between 2200 UTC 9 April 2009 and 0100 UTC 10 April 2009, and the air mass was persistently drier at MAF during the 64-h sample period. Analyses of these two meteorological parameters alone (wind speed and RH), which traditionally constitute National Weather Service Red Flag warning criterion (Lindley et al. 2011), suggest that fire conditions were more severe in the MAF vicinity of west Texas, well west of the wildfire outbreak.

Analyses of RAWS sampled fuel moisture additionally support the false conclusion of a more favorable fire environment in west Texas, with fuel moisture values at MAF that ranged from 3.1% to 4.7% throughout the 64-h period (Fig. 24). Comparatively, fuel moisture values ranged between 5.6% and 9.6% along the LLTR at LBJ. During the diurnal burn period of 9 April 2009, fuel moisture fell to 5.9% at LBJ by

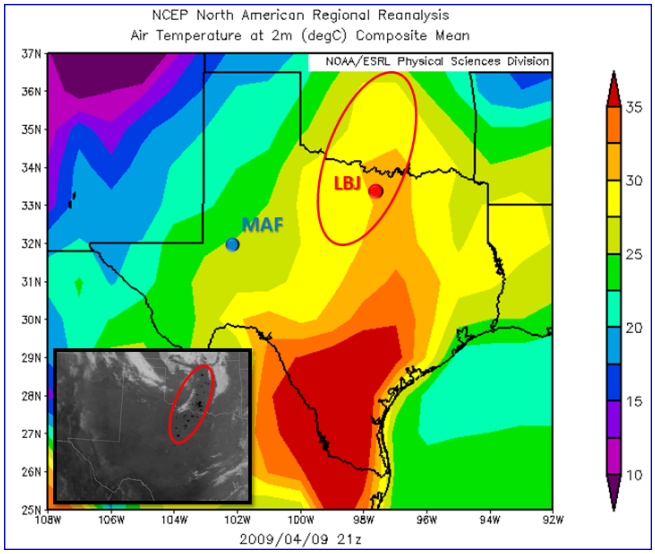


**Figure 21**. NCEP/NARR 2-m temperature showing the LLTR valid 2100 UTC 9 April 2009 and location of the LBJ and MAF RAWS sites. The fire outbreak area is circled (red) and illustrated with SWIR (inset).

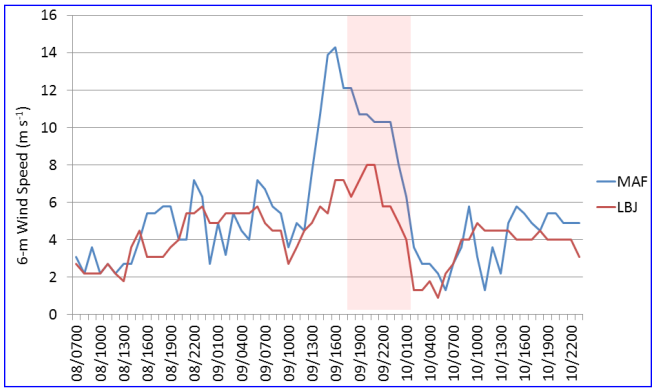


**Figure 22**. RAWS 6-m wind speed measured at MAF and LBJ between 0700 UTC 8 April 2009 and 2200 UTC 10 April 2009. Timeframe of the 9 April 2009 SGPWO is highlighted.

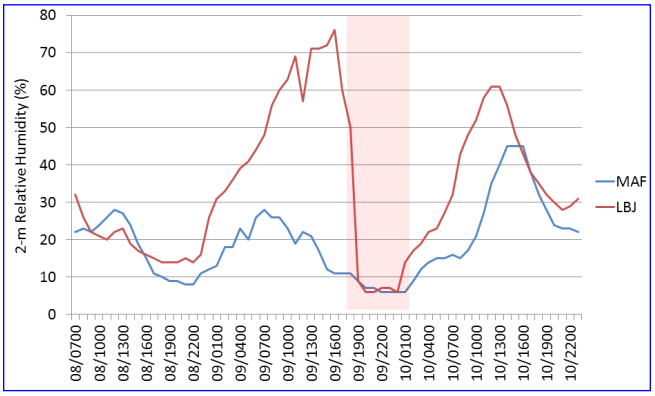


**Figure 23**. RAWS 2-m RH measured at MAF and LBJ between 0700 UTC 8 April 2009 and 2200 UTC 10 April 2009. Timeframe of the 9 April 2009 SGPWO is highlighted.

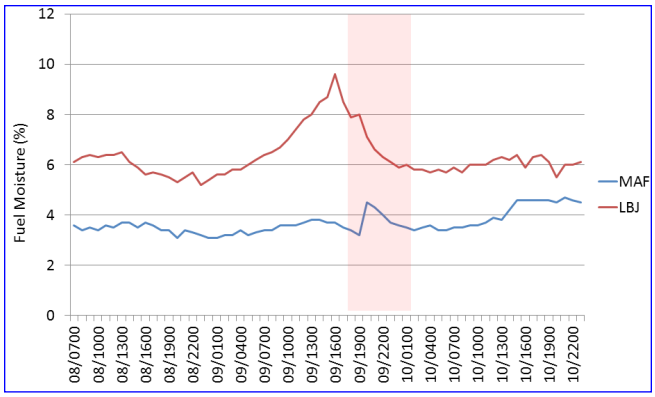


**Figure 24**. RAWS fuel moisture measured at MAF and LBJ between 0700 UTC 8 April 2009 and 2200 UTC 10 April 2009. Timeframe of the 9 April 2009 SGPWO is highlighted.

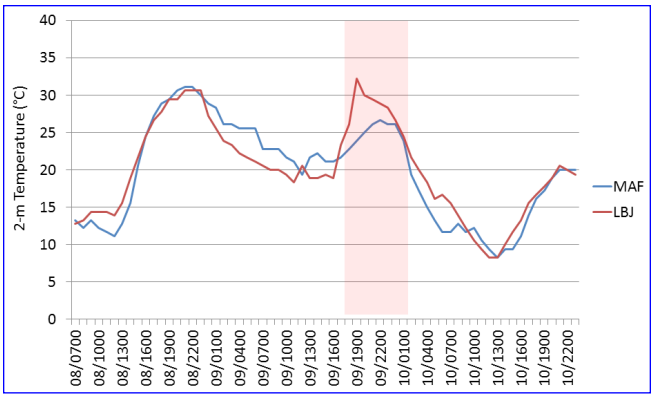


**Figure 25**. RAWS 2-m temperature measured at MAF and LBJ between 0700 UTC 8 April 2009 and 2200 UTC 10 April 2009. Timeframe of the 9 April 2009 SGPWO is highlighted.

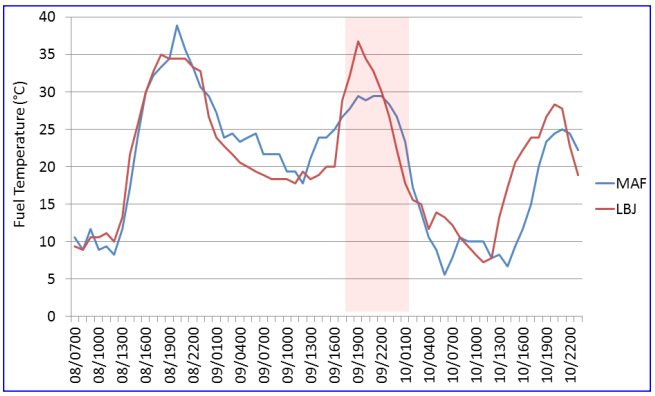


**Figure 26**. RAWS 2-m temperature measured at MAF and LBJ between 0700 UTC 8 April 2009 and 2200 UTC 10 April 2009. Timeframe of the 9 April 2009 SGPWO is highlighted.

0000 UTC 10 April 2009, but corresponding fuel moisture readings at MAF of 3.6% appeared even more critical.

At the time of the fires on 9 April 2009, the only meteorological signals observed by the ROMAN RAWS suggestive of a more fire-effective environment at LBJ versus MAF were found in measures of temperature. A maximum 2-m temperature of 32.2°C occurred at the LBJ RAWS at 1900 UTC on 9 April 2009 (Fig. 25). In comparison, the maximum 2-m temperature at MAF was 26.7°C observed at 2200 UTC on that day. The warmer temperatures observed along the LLTR also were reflected in measures of fuel temperature. Fuel temperature at LBJ peaked at 36.7°C at 1900 UTC, while fuel temperatures at MAF only reached 29.4°C between 1900 UTC and 2200 UTC (Fig. 26). It is worth noting that higher fuel temperatures occurred at MAF during the previous diurnal burn period and reached a maximum of 38.9°C at 2000 UTC on 8 April 2009. Although a daytime minimum 2-m RH of 8% also was observed in association with these conditions, phasing of the key thermodynamic and kinematic features documented in this study did not exist, and 6-m winds only reached sustained speeds of 7.2 m $s^{-1}$. The higher fuel temperatures observed at MAF on 8 April 2009 were not associated with damaging fires. It is hypothesized that the meteorological signals observed in this case emphasize the importance of combined contributions from low- to mid-tropospheric wind maxima, deep mixing, and isentropic coupling that influence environmental fire-effectiveness in proximity to LLTRs. This comparison illustrates how wildland fire behavior and spread become more problematic as strong winds, dry air, and anomalously warm temperatures phase during the interaction of LLTRs and overspreading midlevel wind maxima.

## 5. Conclusions

Analogous to the well-documented fire-effectiveness of WCTTs in the Pacific Northwest, low-level tropospheric thermal ridges enhance wildland fire activity on the southern Great Plains. This study uses both the NARR and NCEP/NCAR Reanalysis to analyze and composite atmospheric conditions for 11 fire-effective LLTRs associated with widespread and damaging wildfire episodes in New Mexico, Texas, and Oklahoma between 2006 and 2014. These analyses show that fire-effective LLTRs occur in proximity to lee surface troughs associated with midlatitude cyclones, and that problematic wildland fire is enhanced when

anomalously strong wind fields aloft overspread a tongue of positive low-level temperature anomalies near the interface of the parent cyclone's warm sector dry/moist boundary. Dangerous wildfire conflagrations frequently occur along and on the windward side of 2-m and 850-hPa thermal ridges. This is where deep boundary layer mixing and isentropic downglide couple to result in fire-effective processes as the LLTR is overspread by an upstream midlevel wind maximum. Conceptual models for identifying fire-effective interactions between LLTRs and wind maxima aloft have proven useful in operational predictions for high-impact wildland fire episodes. Further, comparatively hot air and fuel temperatures observed in proximity to an LLTR-associated wildfire outbreak in Texas and Oklahoma on 9 April 2009 appeared to be the only distinguishable meteorological signal useful in differentiating non-fire-effective and fire-effective environments. During this particular fire episode, traditional measures of fire weather (RH and wind) suggested that conditions were equally, or even more, critical in the core of the dry air mass well west of the LLTR where wildfires did not occur.

Future work should focus on improved operational application of fire-effective LLTRs. Knowledge and recognition of fire-effective LLTRs may prove useful in better identifying truly problematic wildland fire environments. Just as important, recognizing the lack of fire-effective LLTRs is expected to help reduce Red Flag warning false alarms in dry and windy conditions mitigated by relatively cooler temperatures that lead to reduced wildland fire danger. Additional research also is needed to refine wildland fire predictions for a less synoptically evident variant wildfire scenario characterized by broad zones of positive temperature anomalies coupled with strong MSLP gradient-induced surface winds within a relatively moist environment east of the dryline and analyzed LLTR. Such conditions proved to be fire-effective in the timbered fuel regime of eastern Oklahoma on 18 February 2016 and 17 November 2016 and present a significant challenge for predictive service. To fully understand the physical processes that result in greater fire-effectiveness along and near LLTRs, higher resolution sampling of atmospheric and fuel conditions is needed. It is hoped that established meteorological mesonetworks can be leveraged in the future to provide more detailed in-situ observations of the LLTR fire environment.

*Acknowledgments*. The authors would like to thank David Andra, Scott Curl, and Matthew Day of the National Weather Service in Norman, Oklahoma; Brian Curran of the National Weather Service in Midland, Texas; John Brost, Eric Howieson, Paul Witsaman, and Greg Patrick of the National Weather Service Southern Region Headquarters in Fort Worth, Texas; Al Pietrycha of the National Weather Service in Pleasant Hill, Missouri; Nicholas Nauslar of the Storm Prediction Center in Norman, Oklahoma; and Robert Rozumalski of the National Weather Service in Boulder, Colorado, as well as the Editor and three reviewers.

## REFERENCES

Ballentine, R. J., 1980: A numerical investigation of New England coastal frontogenesis. *Mon. Wea. Rev*., **108**, 1479–1497, Crossref.

Baker, D. G., 1971: A study of high pressure ridges to the east of the Appalachian Mountains. Ph.D. thesis, Massachusetts Institute of Technology, 127 pp. [Available online at dspace.mit.edu/bitstream/handle/1721.1/37179/30115495-MIT.pdf?sequence=2.]

Benjamin, S. G., and Coauthors, 2016: A North American hourly assimilation and model forecast cycle: The Rapid Refresh. *Mon. Wea. Rev*., **144**, 1669–1694, Crossref.

Bell, G. D., and L. F. Bosart, 1988: Appalachian cold-air damming. *Mon. Wea. Rev*., **116**, 137–161, Crossref.

Bosart, L. F., 1975: New England coastal frontogenesis. *Quart. J. Roy. Meteor. Soc*., **101**, 957–978, Crossref.

____, 1981: The President's Day snowstorm of 18–19 February 1979: A subsynoptic-scale event. *Mon. Wea. Rev*., **109**, 1542–1566, Crossref.

____, C. J. Vaudo, and J. H. Helsdon, Jr., 1972: Coastal frontogenesis. *J. Appl. Meteor*., **11**, 1236–1258, Crossref.

Brewer, M. C., and C. F. Mass, 2012: The west coast thermal trough: Climatology and synoptic-evolution. *Mon. Wea. Rev*., **140**, 3820–3843, Crossref.

Carlson, T. N., and F. H. Ludlam, 1968: Conditions for the occurrence of severe local storms. *Tellus*, **20**, 203–226, Crossref.

Colson, D., 1956: Meteorological problems associated with mass fires. Fire Control Notes, 17, 9–11. [Available online at www.fs.fed.us/fire/fmt/fmt_pdfs/fmt64-1.pdf.]

Cramer, O. P., 1954: Recognizing weather conditions that affect forest fire behavior. *Fire Control Notes*, **15**, 1–6. [Available online at https://www.fs.fed.us/fire/fmt/fmt_pdfs/015_02.

____, 1957: Frequency of dry east winds over northwest Oregon and southwest Washington. Pacific Northwest Forest & Range Experiment Station, Research Paper 24, 19 pp. [Available online at archive.org/stream/frequencyofdryea24cram#page/n1/mode/2up.]

Doyle, J. D., and T. T. Warner, 1990: Mesoscale coastal processes during GALE IOP 2. *Mon. Wea. Rev*., **118**, 283–308, Crossref.

Forbes, G. S., R. A. Anthes, and D. W. Thomson, 1987: Synoptic and mesoscale aspects of an Appalachian ice storm associated with cold-air damming. *Mon. Wea. Rev*., **115**, 564–591, Crossref.

Gisborne, H. T., 1927: Meteorological factors in the Quartz Creek forest fire. *Mon. Wea. Rev*., **55**, 56–60, Crossref.

Horel, J., M. Splitt, J. Pechmann, B. Olsen, and E. Delgado, 2004: ROMAN - Realtime Observation Monitoring and Analysis Network. *20th Inter. Conf. on Interactive Information and Processing Systems (IIPS) for Meteorology, Oceanography, and Hydrology*, Seattle, WA, Amer. Meteor. Soc., 9.10. [Available online at ams.confex.com/ams/84Annual/techprogram/paper_70125.htm.]

Hobbs, P. V., J. D. Locatelli, and J. E. Martin, 1996: A new conceptual model for cyclones generated in the lee of the Rocky Mountains. *Bull. Amer. Meteor. Soc*., **77**, 1169–1178, Crossref.

Jensen, S. E., and G. R. McPherson, 2008: *Living with Fire: Fire Ecology and Policy for the Twenty-first Century*. University of California Press, 192 pp.

Kalnay, E., and co-authors, 1996: The NCEP/NCAR 40-year reanalysis project. *Bull. Amer. Meteor. Soc*., **77**, 437–471, Crossref.

Keshishian, L. G., and L. F. Bosart, 1987: A case study of extended East Coast frontogenesis. *Mon. Wea. Rev*., **115**, 100–117, Crossref.

____, ____, and W. E. Bracken, 1994: Inverted troughs and cyclogenesis over interior North America: A limited regional climatology and case studies. *Mon. Wea. Rev*., **122**, 565–607, Crossref.

Lindley, T. T., J. D. Vitale, W. S. Burgett, and M.-J. Beierle, 2011: Proximity meteorological observations for wind-driven grassland wildfire starts on the southern High Plains. *Electronic J. Severe Storms Meteor*., **6**, 1–27. [Available online at www.ejssm.org/ojs/index.php/ejssm/article/view/67/61.]

____, and Coauthors, 2014: Southern Great Plains wildfire outbreaks. *Electronic J. Severe Storms Meteor*., **9**, 1–43. [Available online at www.ejssm.org/ojs/index.php/ejssm/article/view/132/98.]

Mesinger, F., and Coauthors, 2006: North American Regional Reanalysis. *Bull. Amer. Meteor. Soc*., **87**, 343–360, Crossref.

Miller, J. E., 1946: Cyclogenesis in the Atlantic coastal region of the United States. *J. Meteor*., **3**, 31–44, Crossref.

Peterson, R. E., 1983: The west Texas dryline: Occurrence and behavior. Preprints, *13th Conf. on Severe Local Storms*, Tulsa, OK, Amer. Meteor. *Soc*. 9–11.

Pierrehumbert, R. T., 1986: Lee cyclogenesis. Mesoscale Meteorology and Forecasting, P. S. Ray, Ed., *Amer. Meteor. Soc*., 493–515, Crossref.

Richwien, B. A., 1980: The damming effect of the southern Appalachians. Natl. Wea. Dig., 5, 2–12. [Available online at nwafiles.nwas.org/digest/papers/1980/Vol05No1/1980v005no01-Richwein.pdf.]

Schaefer, J. T., 1973: The motion and morphology of the dryline. NOAA Tech. Memo ERL NSSL-66, 81 pp. [NTIS No. COM-74-10043.]

____, 1986: The dryline. Mesoscale Meteorology and Forecasting, P. S. Ray, Ed., *Amer. Meteor. Soc*. 549–572, Crossref.

Schumacher, P. N., G. Frosig, M. L. Selzler, and R. A. Weisman, 2008: Precipitation regimes during cold-season central U. S. inverted trough cases. Part II: A composite case study. *Wea. Forecasting*, **23**, 617– 643, Crossref.

Scott, A. C., D. M. J. S. Bowman, W. J. Bond, S. J. Pyne, and M.E. Alexander, 2014: *Fire on earth: An introduction*. John Wiley & Sons, Ltd., 434 pp.

Steenburgh, W. J., and C. F. Mass, 1994: The structure and evolution of a simulated Rocky Mountain lee trough. *Mon. Wea. Rev*., **122**, 2740–2761, Crossref.

Syverson, C. E., 1963: Fire weather synoptic types of the Northern Intermountain, Northern Rockies and the Northwestern Plains Regions. Unpublished report. U. S. Department of Agriculture, Forest Service, Pacific Wildland Fire Sciences Laboratory, Seattle, Washington.

Weisman, R. A., K. G. McGregor, D. R. Novak, J. L. Selzler, M. L. Spinar, B. C. Thomas, and P. N. Schumacher, 2002: Precipitation regimes during cold-season central U. S. inverted trough cases. Part I: Synoptic climatology and composite study. *Wea. Forecasting*, **17**, 1173–1193, Crossref.

Werth, P., and R. Ochoa, 1993: The evaluation of Idaho wildfire growth using the Haines Index. *Wea. Forecasting*, **8**, 223–234, Crossref.

____, and Coauthors, 2011: Synthesis of knowledge of extreme fire behavior: Volume 1 for fire managers. Gen. Tech. Rep. PNW-GTR-854. U. S. Department of Agriculture, Forest Service, Pacific Northwest Research Station, Portland, OR, 144 pp. [Available online at www.met.sjsu.edu/~clements/pnw_gtr854.pdf.]

____, and Coauthors, 2016: Synthesis of knowledge of extreme fire behavior: Volume 2 for fire behavior specialists, researchers, and meteorologists. Gen. Tech. Rep. PNW-GTR-891. U. S. Department of Agriculture, Forest Service, Pacific Northwest Research Station, Portland, OR, 258 pp.